MATERIALS PHYSICS AND MECHANICS RESEARCH ARTICLE

Submitted: September 19, 2025 **Revised: March 5, 2026** **Accepted: April 2, 2026**

Wave reflection analysis in nonlocal porous thermoelastic media under hyperbolic two-temperature and higher-order Green-Lindsay models

S. Sharma [1], D. Batra [2]✉, R. Kumar [3]

[1] Houston University, Houston, USA

[2] Kishan Lal Public College, Rewari, Haryana, India

[3] Kurukshetra University, Kurukshetra, Haryana, India

✉ divya@klpcollege.ac.in

ABSTRACT

The reflection behavior of plane waves in a nonlocal porous thermoelastic half-space incorporating hyperbolic two-temperature effects under impedance boundary conditions within the framework of refined the Green-Lindsay theory is investigated. The formulation accounts for nonlocal elasticity, thermal relaxation, and porous interactions, leading to the propagation of four distinct wave modes, namely primary, thermal, porous, and shear vertical waves, each with different phase velocities. Reflection coefficients are derived analytically, and corresponding energy ratios are computed to examine the influence of hyperbolic two-temperature, two-temperature, and one-temperature models, as well as comparisons between the refined Green–Lindsay and simple Green–Lindsay theories. Numerical results reveal strong sensitivity of energy partition to both angle of incidence and thermal parameters. In particular, hyperbolic two-temperature effects significantly modify energy distribution, leading to pronounced deviations from classical the one-temperature model predictions, especially for primary and shear vertical waves incidences. The refined Green–Lindsay model consistently produces higher and more stable energy ratios compared to the simple Green–Lindsay model, indicating improved representation of thermo-mechanical coupling and relaxation effects. Oscillatory behaviour is observed in several reflected energy components, highlighting the combined influence of nonlocality and thermal phase lags on wave interactions. The results demonstrate that the inclusion of hyperbolic two-temperature and nonlocal effects provides a more refined and physically consistent description of wave propagation in porous media. These findings are of practical importance in applications such as soil mechanics, geophysics, and civil engineering, where accurate prediction of wave reflection and energy distribution under thermal loading conditions is essential.

KEYWORDS

porous medium • reflection • impedance boundary • amplitude ratios • energy ratios

Citation: Sharma S, Batra D, Kumar R. Wave reflection analysis in nonlocal porous thermoelastic media under hyperbolic two-temperature and higher-order Green-Lindsay models. *Materials Physics and Mechanics*. 2026;54(3): 64–84.
http://dx.doi.org/10.18149/MPM.5432026_6

Introduction

Biot [1,2] was the first one who presented the theoretical framework to study the propagation of waves in fluid saturated porous material having low frequency and high frequency range. Following his model many researchers have contributed their work in context of propagation of waves in fluid saturated porous thermoelastic media due to its numerous applications in field of ocean engineering, geophysics, soil engineering etc. The coupled theory of thermoelasticity proposed by Biot [3] has some limitations as in

© S. Sharma, D. Batra, R. Kumar, 2026.
Publisher: Peter the Great St. Petersburg Polytechnic University
This is an open access article under the CC BY-NC 4.0 license (https://creativecommons.org/li-censes/by-nc/4.0/)

case of short work time it is difficult to maintain thermal equilibrium. To overcome this problem two well-known theories of thermoelasticity known as the Lord-Shulman theory [4] (LS theory) and the Green-Lindsay theory [5] (GL theory) drew the attention of researchers over past some decades. These theories predict the finite speed of heat propagation and are known as generalized theories of thermoelasticity. An exact solution for classical coupled thermoporoelasticity in case of cylindrical and spherical coordinates are given by Jabbari and Dehbani [6,7].

Eringen [8] introduced that in non-local theory of elasticity the stress tensor at a point within a continuous body gets influenced by strain at that point as well as the strains at other points of the continuous body also. Non-local stress forces act as a remote action force, and such types of forces are dealt with in study of atomic theory of lattice dynamics. In nonlocal theory of elasticity, small scale parameters are introduced in the constitutive equations to represent the atomic distance. Such type of nonlocal continuum mechanics is widely used to study the wave propagation problems [9–14]. Sharma and Marin [15,16] studied some problems on reflection of waves in micropolar thermoelastic medium. Sharma and Sharma [17] employed Laplace and Hankel transformation to study the impact of temperature fluctuations on tissues. Reflection parameters are strongly influenced by the diffusion parameters as compared to electric and magnetic parameters in GL model [18]. Abo-Dahab [19] obtained the reflection and transmission coefficients of waves at the solid-liquid interface and studied the effect of magnetic and initial stress on them in context of generalized theory of GL model. Othman and Ahmed [20] applied GL theory to study the deformation of piezothermoelastic medium with rotation under the impact of gravity.

Lofty and Gabr [21] employed LS, GL and couple theory to study the effect of mechanical force in semiconducting infinite medium with two-temperatures. Abo-Dahab [22] used Lame's potential method in context of LS theory and investigated the impact of magnetic field on reflection of waves in a thermoelastic half space with two temperatures. Dahab et al. [23] presented that in case of two temperatures the behavior of particles is more realistic than one temperature generalized thermoelastic medium and it has strong impact on reflection coefficients. Saeed et al. [24] used finite element method to study the impact of thermal relaxation times on poroelastic materials in context of GL model. Anaya and Khan [25] used GL theory to study the reflection of thermoelastic waves in a rotating fiber reinforced medium with magnetic field. The effect of nonlocal, micropolar and rotation parameters on reflection coefficients from micropolar thermoelastic medium is studied by Kalkal et al. [26]. Sharma and Khator [27,28] studied some problems on power generation using renewable energy sources. An intensive study in context of higher order derivatives with nonlocal parameters in micropolar thermoelastic media is presented in works of [29–31]. The nonlocal parameters in rotating fractional order porous medium have no impact on quasi void wave [32]. Reflection of waves in an orthotropic micropolar thermoelastic diffusive medium having two temperatures is studied by Punia et al. [33]. Kumar et al. [34] employed the Moore-Gibson-Thompson heat equation to under hyperbolic two-temperatures to study the deformation in an axisymmetric micropolar thermoelastic medium. Kaushal et al. [35] studied the behavior of waves propagating in a non-local thermoelastic medium using modified the Green and Lindsay model having impedance boundary conditions.

Abouelregal [36] used modified higher order thermoelasticity and studied the effect of micropolarity, phase delay and nonlocal index on micropolar viscoelastic nanostructures subject to laser induced heat flux. Sharma et al. [37] analyzed wave motion in fractional order swelling porous thermoelastic medium having impedance boundary conditions. Sharma et al. [38] studied the reflection of plane waves in porothermoelastic half space having three phase lags. Sharma et al. [39] used chemical potential sources and studied thermal and chemical responses on nonlocal thermoelastic diffusive half-space. Marin et al. [40] examined the fundamental sol and Green's function in photothermelastic under MGT heat equation and temperature dependent properties. Kumar et al. [41] examined the influence of viscosity on energy ratios at boundary involving elastic and piezothermoelastic with two temperature and phase lags. Abouelregal et al. [42] proposed a spatiotemporal nonlocal model and highlighted the importance of size dependent higher order derivative to study the temporal nonlocal effects in micropolar viscoelastic medium exposed to short-pulse laser excitation. Later, in [43], it was introduced the groundbreaking dual phase lag theroy of thermoelasticity and bridges the gap between traditional continuum mechanics and nanoscale mechanics. A novel thermoelastic model developed by integrating nonlocal theory of elasticity, the Kelvin-Voigt viscoelastic model and the Klein-Gordon type nonlocal model of elasticity in proposed in works of Abouelregal et al. [44]. In [45], it was also used a two-parameter Mittag-Leffler kernel and provided a more precise framework to analyse the complex interactions of porous structures.

In the present paper, reflection of plane waves in a nonlocal porous thermoelastic half-space in context of refined the Green and Lindsay model (RGL) and the simple Green and Lindsay model (SGL) are studied. Existence of three longitudinal waves i.e. primary wave (P-wave), thermal wave (T-wave), porous wave (Ps-wave) and one transversal waves (SV-wave) moving with distinct velocities is studied. Impedance boundary conditions are imposed to obtain the reflection coefficients due to incidence of each wave. Using these reflection coefficients energy ratios are computed for hyperbolic two-temperature (HTT), two-temperature (TT) and one-temperature (1T) cases. Energy ratios are also calculated for RGL and SGL models and it is observed that RGL model gives more refined results than SGL model. Results obtained may be useful in field of soil mechanics and civil engineering.

Basic equations

The field equations in an incompressible porous thermoelastic medium in absence of heat sources and body forces are Jabbari and Dehbani [7] and Abouelregal et al. [44] as:

$$(\lambda+\mu)\nabla\nabla\vec{u}+\mu\nabla^2\vec{u}-\alpha\nabla P-\beta\left(1+\delta_{2m}\sum_{n=1}^{N}\tau_1^n\frac{\partial^n}{\partial t^n}\right)\nabla T=\rho\left(1-l^2\nabla^2+\tau^2\frac{\partial^2}{\partial t^2}\right)\frac{\partial^2\vec{u}}{\partial t^2}, \tag{1}$$

$$\frac{K^o}{\gamma_w}\nabla^2P-\alpha_p\dot{P}-Y\dot{T}-\alpha\nabla\dot{\vec{u}}=0, \tag{2}$$

$$K\nabla^2\varphi=\left(1+\sum_{n=1}^{N}\tau_0^n\frac{\partial^n}{\partial t^n}\right)\left[ZT_0\dot{\mathrm{T}}-YT_0\dot{\mathrm{P}}\right]+\beta T_0\nabla\dot{\vec{u}}, \tag{3}$$

$$\ddot{T}=(\ddot{\varphi}-\beta^*\nabla^2\varphi), \tag{4}$$

where λ and μ are the Lame's constants of the solid skeleton, $\vec{u}$ is a displacement vector of the solid matrix, $\alpha=1-\frac{C_s}{C}$ is the Biot's constant, $C=\frac{3(1-2\nu)}{E}$ is a coefficient of

volumetric thermal expansion of the solid body, C_s=$\frac{3(1-2\nu_s)}{E_s}$ is weight loss in solid grain, $\beta = \frac{3\alpha_s}{C}$ is change in temperature, α_s is a rate of straight-line heat expansion in solid grain's, φ is a porosity of weight fraction of pores in the solid grains, ρ is a mass density of the solid matrix, P is a pore fluid pressure, T_0 is the initial uniform temperature of the medium, T is a temperature change from the reference temperature, K^o is a hydraulic conductivity, α_w is a pore water linear thermal expansion, γ_w is an unit for pore water, α_p=$n(C_w$-$C_s)\alpha C_s$, C_w is a pore water volumetric compression, ρ_s is density of solid grains, ρ_w is a density of pore water, E is the Young's modulus of the elastic solid matrix, K is a thermal conductivity of the porous medium, υ is Poisson's ratio of the solid skeleton, τ_0 and τ_1 thermal relaxation times in the Green-Lindsay thermoelastic model, representing finite speed heat propagation effects, l and τ are the non-local characteristic length parameters that accounts for small-scale (long-range) interactions in the nonlocalelasticity theory, e_{kl} is a strain tensor components, β^* is HTT parameter, k_i is wave numbers corresponding to different wave modes, ω is an angular frequency of the propagating wave, Y=$3(n\alpha_w+(\alpha$-$n)\alpha_s)$, α_p=$n(C_w$-$C_s)\alpha C_s$, Z=$\frac{(1-n)\rho_s C_s+n\rho_w C_w}{T_0}$, Z_1, Z_2, Z_3, Z_4 are impedance parameters at the boundary.

The constitutive relation following Jabbari and Dehbani [6] is taken as:

$$t_{kl} = (\lambda e_{kk} - \beta T - \alpha P)\delta_{kl} + 2\mu e_{kl}, \quad (5)$$

where $e_{kl} = \frac{1}{2}(u_{k,l} + u_{l,k})$, k,l = 1,2,3.

In Eq. (1), δ_{2m} denotes the Kronecker delta function, defined as δ_{2m}=1 when m=2 and δ_{2m}=0 otherwise. The parameter m is introduced to distinguish between different generalized thermoelastic models within a unified mathematical formulation. Specifically, m = 1 corresponds to the Lord-Shulman (LS) thermoelastic model, which involves a single thermal relaxation time, whereas m = 2 corresponds to the Green-Lindsay (GL) thermoelastic model, which incorporates two thermal relaxation times. The parameter N represents the number of relaxation-related terms included in the generalized formulation. The presence of the factor δ_{2m} ensures that the additional relaxation contribution appears only for the GL model and vanishes in the LS model. This formulation allows both thermoelastic theories to be expressed within a single set of governing equations.

Geometry of the problem

A homogeneous, isotropic, porous thermoelastic half-space incorporating non-local and two-temperature effects is considered. A rectangular Cartesian coordinate system $0x_1x_2x_3$ is chosen such that the wave front remains parallel to the x_2 axis, with propagation occurring within the x_1-x_3 plane, and the x_3 - axis oriented perpendicular to the surface of the medium. The complete geometry of the problem is explained with the help of Fig. 1. The components of displacement in two dimensions are:

$$\vec{u} = (u_1, 0, u_3). \quad (6)$$

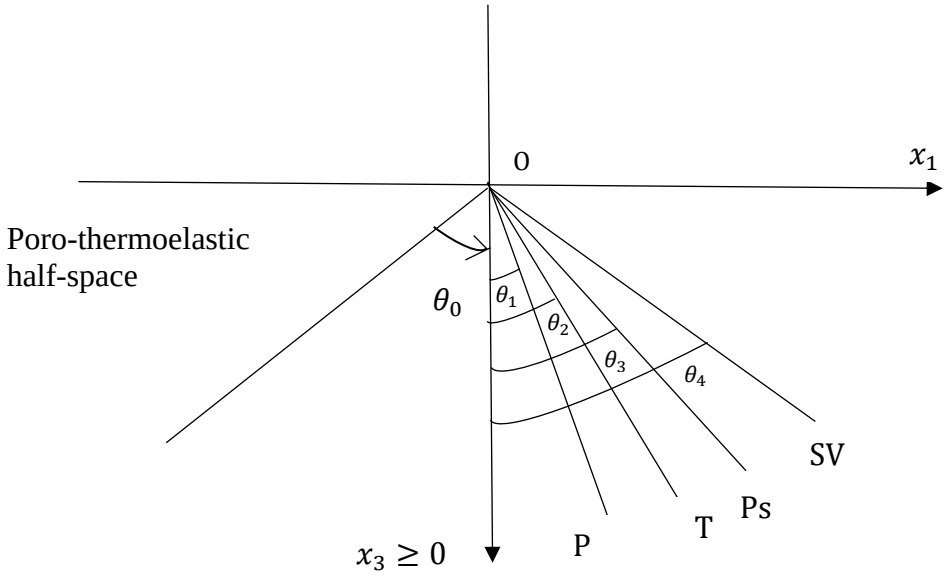


Fig. 1. Geometrical structure of the problem

The dimensionless expressions are defined as:

$$(x_i', u_i', l', \zeta^{*'}) = \frac{\omega_1}{c_1}(x_i, u_i, l, \zeta^*), (P', t_{ij}') = \frac{1}{\beta T_0}(P, t_{ij}),$$
$$(t', \tau_0', \tau') = \omega_1(t, \tau_0, \tau), \beta^{*\prime} = \frac{\omega_1^2}{c_1^2},\ (\varphi', T') = \frac{1}{T_0}(\varphi, T), \omega_1 = \frac{ZT_0c_1^2}{K},\ c_1^2 = \frac{\lambda+2\mu}{\rho}, \quad (7)$$
$$(Z_1', Z_2') = \frac{c_1}{\beta T_0}(Z_1, Z_2), Z_3' = \frac{c_1}{K}Z_3, Z_4' = \frac{c_1}{K^o}Z_4.$$

Using Helmholtz representation, displacement components $u_1(x_1, x_3, t)$ and $u_3(x_1, x_3, t)$ in terms of the scalar potential functions $\Phi(x_1, x_3, t)$ and $\psi(x_1, x_3, t)$ are given by:

$$u_1 = \frac{\partial\Phi}{\partial x_1} - \frac{\partial\psi}{\partial x_3}, u_3 = \frac{\partial\Phi}{\partial x_3} + \frac{\partial\psi}{\partial x_1}. \quad (8)$$

Using Eqs. (6)–(8) in Eqs. (1)–(4) and after restraining primes we obtain:

$$\left(\nabla^2 - (1 - l^2\nabla^2 + \tau^2\frac{\partial^2}{\partial t^2})\frac{\partial^2}{\partial t^2}\right)\Phi - a_1P - a_2\left(1 + \sum_{n=1}^{N}\tau_1^n\frac{\partial^n}{\partial t^n}\right)T = 0, \quad (9)$$
$$\nabla^2\dot{\Phi} - a_3\nabla^2P + a_4\dot{P} + a_5\dot{T} = 0, \quad (10)$$
$$\nabla^2\varphi = b_1\left(1 + \sum_{n=1}^{N}\tau_0^n\frac{\partial^n}{\partial t^n}\right)\dot{T} - b_2\left(1 + \sum_{n=1}^{N}\tau_0^n\frac{\partial^n}{\partial t^n}\right)\dot{P} + b_3\nabla^2\dot{\Phi}, \quad (11)$$
$$\delta_1^2\nabla^2\psi = (1 - l^2\nabla^2 + \tau^2\frac{\partial^2}{\partial t^2})\frac{\partial^2\psi}{\partial t^2}, \quad (12)$$
$$\ddot{T} = (\ddot{\varphi} - \beta^*\nabla^2\varphi), \quad (13)$$

where $a_1 = \frac{\alpha\beta T_0}{\lambda+2\mu}, a_2 = \frac{\beta T_0}{\lambda+2\mu},\ a_3 = \frac{\beta\omega_1 T_0 K^o}{\alpha c_1^2\gamma_w}, a_4 = \frac{\alpha_p\beta T_0}{\alpha}, a_5 = \frac{YT_0}{\alpha}, b_1 = \frac{c_1^2ZT_0}{\omega_1 K}, b_2 = \frac{\beta c_1^2YT_0}{\omega_1 K}$, $b_3 = \frac{\beta c_1^2}{\omega_1 K}, \delta_1^2 = \frac{\mu}{\lambda+2\mu}$.

Wave propagation analysis

Let us consider a plane wave propagating within a thermoelastic porous solid half-space bounded at $x_3 = 0$. For each incident wave, multiple reflected components are generated, including a longitudinal wave (P-wave), a thermal wave (T-wave), a porous wave (Ps-wave), and a shear vertical wave (SV-wave), as illustrated in Fig. 1.

For a harmonic plane wave propagation, when the wave normal vector lies in x_1-x_3 plane making an angle ϑ_0 with the positive x_3-axis normal to the surface, the solution of Eqs. (9)–(13) is taken as:

(Φ, φ, P, ψ) as $(\bar{\Phi}, \bar{\varphi}, \bar{P}, \bar{\psi})e^{i\{\xi(x_1 sin\theta - x_3 cos\theta) - \omega t\}}$, (14)

where ϑ is the angle of incidence and ξ is the wave number

Upon using Eq. (14) in Eqs. (9)–(11), and with aid of Eq. (13), we obtain:

$(\tau_{11} + \tau_{12}v^2)\Phi + (\tau_{13}v^2 + \tau_{14})\varphi + \tau_{15}v^2 P = 0,$ (15)

$\Phi + (\tau_{21}v^2 + \tau_{22})\varphi + (\tau_{24}v^2 + \tau_{23})P = 0,$ (16)

$\tau_{31}\Phi + (\tau_{32}v^2 + \tau_{33})\varphi + \tau_{34}v^2 P = 0.$ (17)

The characteristic equation obtained for consistent solution of system of equations (15)–(17) is given by:

$E_1 v^6 + E_2 v^4 + E_3 v^2 + E_4 = 0.$ (18)

Equation (12) with aid of Eq. (14) gives:

$v^2 = \frac{\delta_1^2 - l^2\omega^2}{1 - \tau^2\omega^2},$ (19)

where $\tau_{11} = -1 + l^2\omega^2, \tau_{12} = 1 - \tau^2\omega^2, \tau_{13} = \frac{-a_2\left(1+\sum_{n=1}^{N}\tau_1{}^n(-i\omega)^n\right)}{\omega^2}, \tau_{14} = (1 - i\omega\tau_1)\varsigma^* a_2,$
$\tau_{15} = \frac{-a_1}{\omega^2}, \tau_{21} = \frac{-a_5}{\omega^2}, \tau_{22} = a_5\varsigma^*, \tau_{23} = \frac{a_3}{i\omega}, \tau_{24} = \frac{-a_4}{\omega^2}, \ \tau_{31} = \omega^2 b_3 i\omega, \tau_{32} = -i\omega b_1(1 - \ \tau_0 i\omega),$
$\tau_{33} = (-\tau_{32}\varsigma^* + 1)\omega^2, \tau_{34} = \ b_2 i\omega(1 + \sum_{n=1}^{N}\tau_0{}^n(-i\omega)^n), s_{11} = \tau_{21}\tau_{34} - \tau_{32}\tau_{24},$
$s_{12} = \tau_{22}\tau_{34} - \tau_{32}\tau_{23} - \tau_{33}\tau_{24}, s_{13} = -\tau_{33}\tau_{23}, \ s_{21} = \tau_{34} - \tau_{31}\tau_{24}, s_{22} = -\tau_{31}\tau_{23},$
$s_{31} = \tau_{32} - \tau_{31}\tau_{21}, s_{32} = \tau_{33} - \tau_{22}\tau_{31}, E_1 = \tau_{12}s_{11}, E_2 = \tau_{11}s_{11} + \tau_{12}s_{12} - \tau_{13}s_{21} + \tau_{15}s_{31},$
$E_3 = \tau_{11}s_{12} + \tau_{12}s_{13} - \tau_{13}s_{22} - \tau_{14}s_{21} + \tau_{15}s_{32}, E_4 = \tau_{11}s_{13} - \tau_{14}s_{22}, \ a_1 = \frac{\alpha\beta T_0}{\lambda+2\mu}, a_2 = \frac{\beta T_0}{\lambda+2\mu},$
$a_3 = \frac{\beta\omega_1 T_0 K^o}{\alpha c_1^2 \gamma_w}, a_4 = \frac{\alpha_p \beta T_0}{\alpha}, a_5 = \frac{YT_0}{\alpha}, b_1 = \frac{c_1^2 ZT_0}{\omega_1 K}, b_2 = \frac{\beta c_1^2 YT_0}{\omega_1 K}, \ b_3 = \frac{\beta c_1^2}{\omega_1 K}, \delta_1^2 = \frac{\mu}{\lambda+2\mu},$

where $\varsigma^* = \begin{cases} \frac{\beta^*}{\omega^2} & \text{for hyperbolic two} - \text{temperature (HTT)}, \\ a^2 & \text{for two} - \text{temperature (TT)}, \\ 0 & \text{for one temperature (1T)}. \end{cases}$

Making use of Eqs. (6)–(8) in Eq. (5) and with aid of Eq. (13) we obtain:

$t_{33} = h_1\left(\frac{\partial^2\Phi}{\partial x_1^2} + \frac{\partial^2\Phi}{\partial x_3^2}\right) + h_2\left(\frac{\partial^2\Phi}{\partial x_3^2} + \frac{\partial^2\psi}{\partial x_3 \partial x_1}\right) - \alpha P - (1 + \varsigma^*\nabla^2)\varphi,$ (20)

$t_{31} = \frac{h_2}{2}\left(2\frac{\partial^2\Phi}{\partial x_3 \partial x_1} + \frac{\partial^2\psi}{\partial x_1^2} - \frac{\partial^2\psi}{\partial x_3^2}\right),$ (21)

where $h_1 = \frac{\lambda}{\beta T_0}, h_2 = \frac{2\mu}{\beta T_0}.$

Restrictions on boundary

The impedance boundary conditions at $x_3 = 0$ are taken as [46,47]:

(i) $t_{33} + \omega z_1 u_3 = 0,$
(ii) $t_{31} + \omega z_2 u_1 = 0,$
(iii) $K\frac{\partial\varphi}{\partial x_3} + \omega z_3\varphi = 0,$ (22)
(iv) $K^o\frac{\partial P}{\partial x_3} + \omega z_4 P = 0,$

where z_1 are z_2 are the impedance parameters having dimension $\frac{Ns}{m^3}$, z_3 and z_4 are also impedance factors having dimensions $\frac{N}{mK}$ and $\frac{N}{m^3 s}$, respectively. The values of Φ, φ, P, and ψ are given by:

$\Phi = \sum A_{0i}e^{i\{\xi_i(x_1 sin\theta_0 - x_3 cos\theta_0) - \omega t\}} + A_i e^{i\{\xi_i(x_1 sin\theta_i + x_3 cos\theta_i) - \omega t\}},$ (23)

$\varphi = \sum \beta_i(A_{0i}e^{i\{\xi_i(x_1 sin\theta_0 - x_3 cos\theta_0) - \omega t\}} + A_i e^{i\{\xi_i(x_1 sin\theta_i + x_3 cos\theta_i) - \omega t\}},$ (24)

$P = \sum \alpha_i(A_{0i}e^{i\{\xi_i(x_1 sin\theta_0 - x_3 cos\theta_0) - \omega t\}} + A_i e^{i\{\xi_i(x_1 sin\theta_i + x_3 cos\theta_i) - \omega t\}},$ (25)

$\psi = B_{04}e^{i\{\xi_4(x_1 sin\theta_0 - x_3 cos\theta_0) - \omega t\}} + B_4 e^{i\{\xi_4(x_1 sin\theta_4 + x_3 cos\theta_4) - \omega t\}},$ (26)

where $\alpha_i = \frac{(\tau_{11}+\tau_{12}V^2)(\tau_{22}+\tau_{21}V^2)-(\tau_{13}V^2+\tau_{14})}{(\tau_{13}V^2+\tau_{14})(\tau_{23}+\tau_{24}V^2)-\tau_{15}V^2(\tau_{22}+\tau_{21}V^2)}$, $\beta_i = \frac{\tau_{15}V^2-(\tau_{11}+\tau_{12}V^2)(\tau_{23}+\tau_{24}V^2)}{(\tau_{13}V^2+\tau_{14})(\tau_{23}+\tau_{24}V^2)-\tau_{15}V^2(\tau_{22}+\tau_{21}V^2)}$, $(i = 1,2,3)$.

The quantities $A_{0i}(i = 1,2,3)$ and B_{04} represent the amplitudes of the incident part of P-wave, T-wave Ps-wave and SV-wave respectively. Similarly, $A_i(i = 1,2,3)$ and B_4 denote the amplitudes of the corresponding reflected P-wave, T-wave, Ps-wave, and SV-wave. According to Snell's law, the relationship between the incident and reflected angles is expressed as $\frac{sin\theta_0}{v_0} = \frac{sin\theta_i}{v_i}$ for $i = 1,2,3,4$.

Furthermore, the wave parameters satisfy the condition: $\xi_1 v_1 = \xi_2 v_2 = \xi_3 v_3 = \xi_4 v_4 = \omega$, where ω is the angular frequency. Using Eqs. (8), (23)–(26) in Eq. (22) the following expressions representing the relation between amplitude coefficients are obtained:

$$\sum a_{pj} Z_j = g_p, (p,j = 1,2,3,4), \tag{27}$$

where $a_{1i} = -\left(h_1 + h_2\left(1-\left(\frac{v_i}{v_1}\right)^2 sin^2\theta_0\right) - \beta^*\beta_i + \frac{\alpha\alpha_i+\beta_i}{\xi_i^2}\right)\left(\frac{v_1}{v_i}\right)^2 + iz_1\frac{v_1^2}{v_i}\sqrt{1-\left(\frac{v_i}{v_1}\right)^2 sin^2\theta_0}$,

$a_{14} = -h_2\frac{v_1}{v_4}sin\theta_0\sqrt{1-\left(\frac{v_4}{v_1}\right)^2 sin^2\theta_0} + iz_1 v_1 sin\theta_0$,

$g_1 = h_1 + h_2 cos^2\theta_0 + \frac{\alpha\alpha_1+\beta_1}{\xi_1^2} + \beta^*\beta_1 + iz_1 v_1 cos\theta_0$,

$a_{2i} = -h_2\frac{v_1}{v_i}sin\theta_0\sqrt{1-\left(\frac{v_i}{v_1}\right)^2 sin^2\theta_0} + iz_2 v_1 sin\theta_0$,

$a_{24} = \frac{h_2}{2}\left(\frac{v_1}{v_4}\right)^2\left(1-2sin^2\theta_0\left(\frac{v_4}{v_1}\right)^2\right) - iz_2\frac{v_1^2}{v_4}\sqrt{1-\left(\frac{v_4}{v_1}\right)^2 sin^2\theta_0}$,

$g_2 = -h_2 sin\theta_0 cos\theta_0 - iz_2 v_1 sin\theta_0$,

$a_{3i} = i\frac{\beta_i}{\xi_i}\left(\frac{v_1}{v_i}\right)^2\sqrt{1-\left(\frac{v_i}{v_1}\right)^2 sin^2\theta_0} + z_3\frac{\beta_i}{\xi_i}\frac{v_1^2}{v_i}, a_{34} = 0, g_3 = i\frac{\beta_1}{\xi_1}cos\theta_0 - \frac{v_1}{\xi_1}z_3\beta_1$,

$a_{4i} = i\frac{\alpha_i}{\xi_i}\left(\frac{v_1}{v_i}\right)^2\sqrt{1-\left(\frac{v_i}{v_1}\right)^2 sin^2\theta_0} + z_4\frac{\alpha_i}{\xi_i}\frac{v_1^2}{v_i}, a_{44} = 0, g_4 = i\frac{\alpha_1}{\xi_1}cos\theta_0 - z_4\frac{\alpha_1}{\xi_1}v_1$.

Here, $Z_i = \frac{A_i}{A_{01}}$ $(i = 1,2,3)$ and $Z_4 = \frac{B_4}{A_{01}}$ reflection coefficients of P-wave, T-wave, Ps-wave and SV-wave respectively corresponding of incidence of P wave. Similarly, reflection coefficients due to the incidence of T-wave, Ps-wave, and SV- wave can be calculated.

Energy ratios

Following [48], the partition of energy is taken as:

$$P^e = \frac{1}{2}\Re(t_{33}\vec{u}_3) + \frac{1}{2}\Re(t_{31}\vec{u}_1). \tag{28}$$

With the help of Eq. (27) the reflected wave energy at $x_3 = 0$ is represented by:

$$|E_i| = -\left(\frac{A_i}{A_{01}}\right)^2\frac{\xi_1\omega cos\theta_1\left[-\xi_1^2\left(\frac{\lambda+2\mu}{\beta T_0}-\beta^*\beta_i\right)+\beta_1+\alpha\alpha_1\right]}{\xi_1\omega cos\theta_0\left[-\xi_1^2\left(\frac{\lambda+2\mu}{\beta T_0}-\beta^*\beta_i\right)+\beta_1+\alpha\alpha_1\right]}, \tag{29}$$

$$|E_4| = -\left(\frac{B_4}{A_{01}}\right)^2\frac{\left(\frac{h_2}{2}\right)\xi_4^3\omega cos\theta_4}{\left(\frac{h_2}{2}\right)\xi_4^3\omega cos\theta_0}. \tag{30}$$

Particular cases

1. By taking $m = 2$ and $N = 3$ in Eqs. (1) and (3), we obtain the results for the refined Green and Lindsay model (RGL).
2. For $m = 2$ and $N = 1$, in basic equations (1) and (3) results correspond to the simple Green and Lindsay model (SGL).

3. Taking $\varsigma^{*}=a^{2}$ yield the results for porous thermoelasticity with two-temperature and non-locality.

Numerical Results

In Figs. 2–9, the horizontal axis represents the angle of incidence θ (in degrees), while the vertical axis shows the dimensionless energy ratios of the reflected waves. The legends distinguish the thermoelastic models considered, namely hyperbolic two temperature (HTT), two-temperature (TT) and one temperature (1T). These figures illustrate the variation of reflected wave energy with the angle of incidence under different thermoelastic conditions. To compute the theoretical results the values of various physical quantities are taken following Jabbari and Dehbani [6] (Table 1).

Table 1. Numerical data for computation

Symbol	Value	Unit	Symbol	Value	Unit
λ	12.50	N/m^2	α_s	0.0051	1/K
μ	8.33	N/m^2	α_w	0.089	1/K
T_0	293.00	K	c_s	2.90	m^2/N
ρ	8.954	Ns^2/m^4	c_w	2.099	m^2/N
K^o	1.70	m^4/N	ρ_s	2.60	Ns^2/m^4
γ_w	0.001	s	ρ_w	1.00	Ns^2/m^4
K	1.50	N/sK	E	1.00	$N/m^2\,K^2$

$n = 0.3, \tau_1 = 0.1, \tau = 0.003,\ l = 0.002.$

Solution of Eqs. (29) and (30) using the given numbers and impedance parameters $z_1 = 10$, $z_2 = 20$, $z_3 = 30$, $z_4 = 40$ we acquire the energy ratios for the reflected *P*-wave, *T*-wave, *Ps*-wave, and *SV*-wave. These are shown in Figs. 2–5.

Impact of ς^{*} on energy ratios

Figures 2–5 demonstrate the impact of ς^{*} on energy ratios for $\varsigma^{*} = 0.06$ (hyperbolic two temperature (HTT)), $\varsigma^{*} = 0.002$ (two temperatures (TT)) and $\varsigma^{*} = 0$ (one temperature (1T)).

P-wave

Figure 2 exhibits the impact of ς^{*} on energy ratios due to incidence of P-wave. Figure 2(a) reveals that in case of HTT and 1T the values of $|E_1|$ are close to each other with little variation in their magnitudes, whereas TT values decrease with angle of incidence and attains least values in the range $\theta \geqslant 33°$. The values of $|E_2|$ increase with angle of incidence. It has highest value in case of 1T and lowest values for TT model. Figure 2(c) shows that TT and 1T follow the same trend for variation of values of $|E_3|$. It initially decreases with angle of incidence and then starts increasing. On contrary to that in case of HTT values decrease with angle of incidence and overcome the outcomes of remaining models. $|E_4|$ increase with higher values of ς^{*} and angle of incidence as represented in Fig. 2(d), whereas $|E_{int}|$ decrease with angle of incidence and has least values in case of 1T.

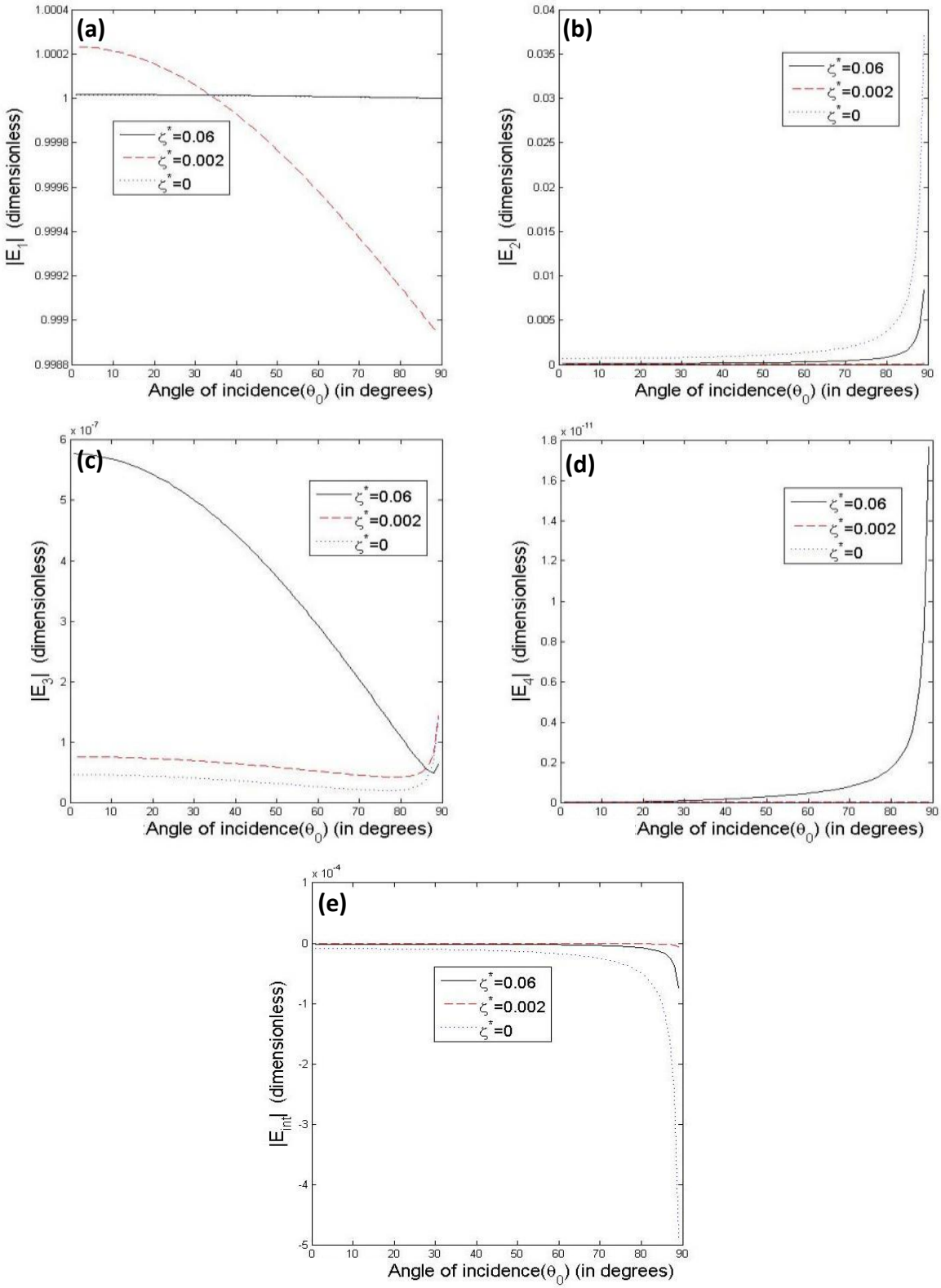


Fig. 2. Energy ratios of reflected wave w.r.t. angle of incidence ((a) $|E_1|$, (b) $|E_2|$, (c) $|E_3|$, (d) $|E_4|$, (e) $|E_{int}|$) for incident P-wave at ς*=0, 0.002, 0.06

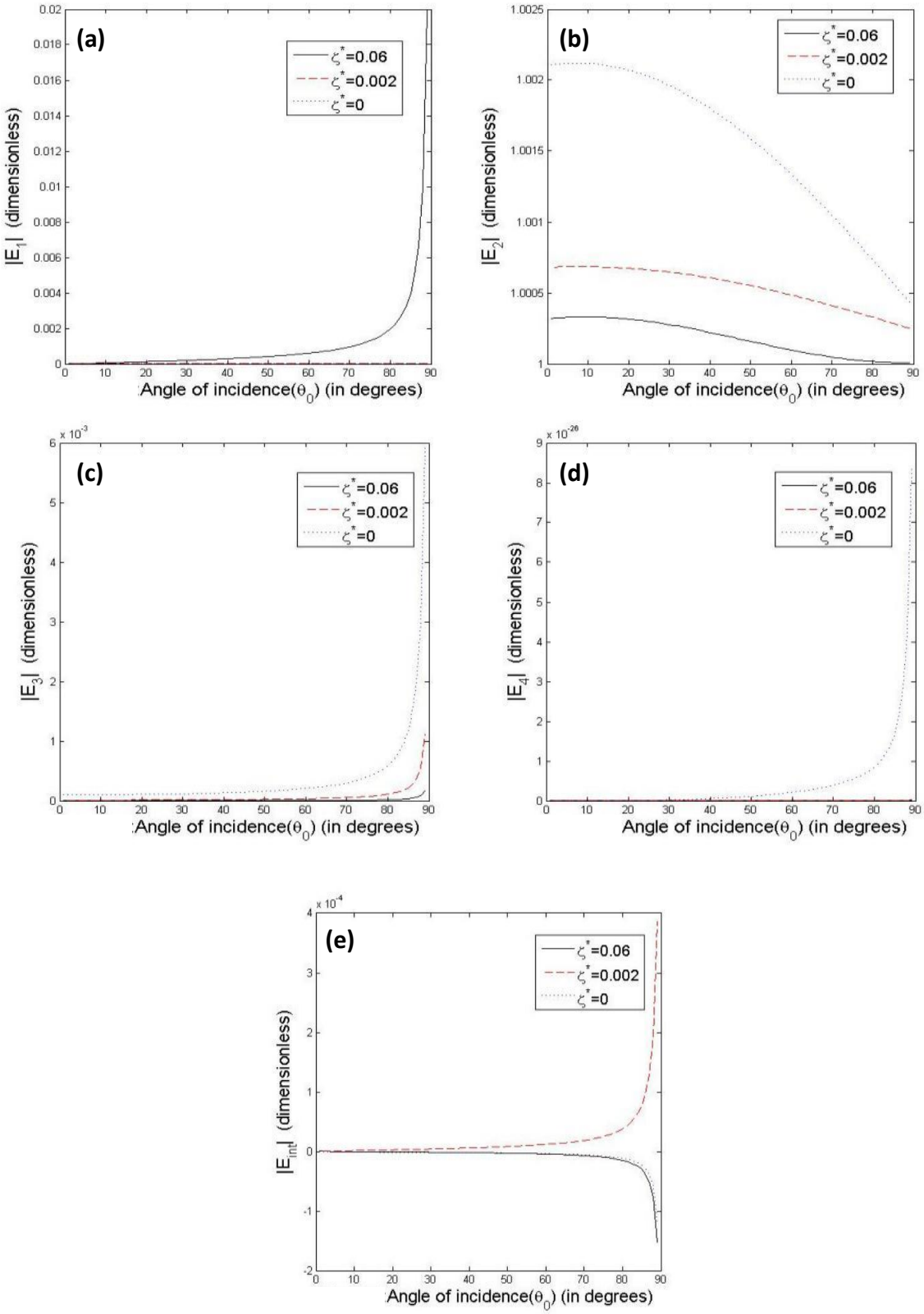


Fig. 3. Energy ratios of reflected wave w.r.t. angle of incidence ((a) $|E_1|$, (b) $|E_2|$, (c) $|E_3|$, (d) $|E_4|$, (e) $|E_{int}|$) for incident T-wave at ς*=0, 0.002, 0.06

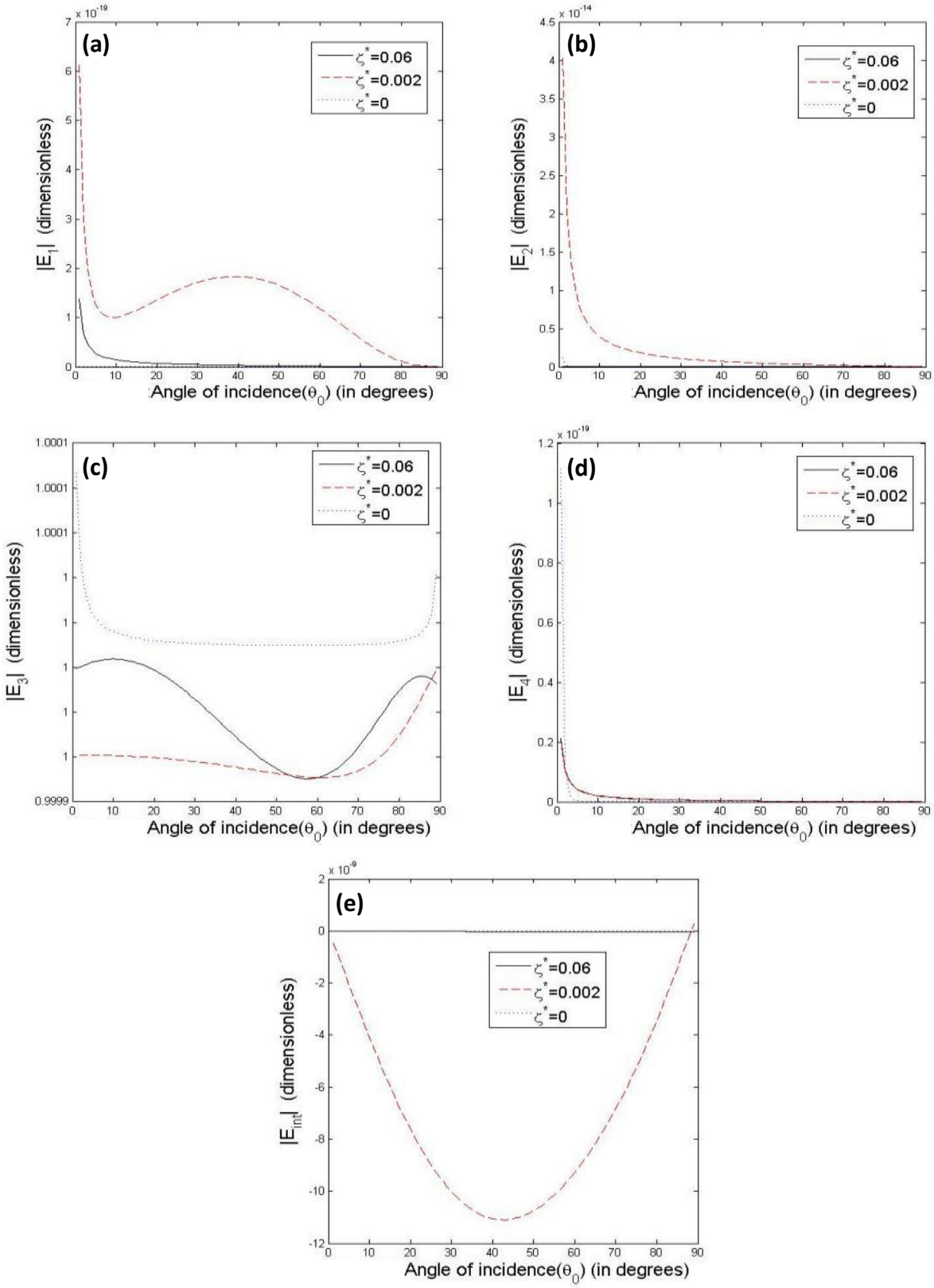


Fig. 4. Energy ratios of reflected wave w.r.t. angle of incidence ((a) $|E_1|$, (b) $|E_2|$, (c) $|E_3|$, (d) $|E_4|$, (e) $|E_{int}|$) for incident Ps-wave at ς^*=0, 0.002, 0.06

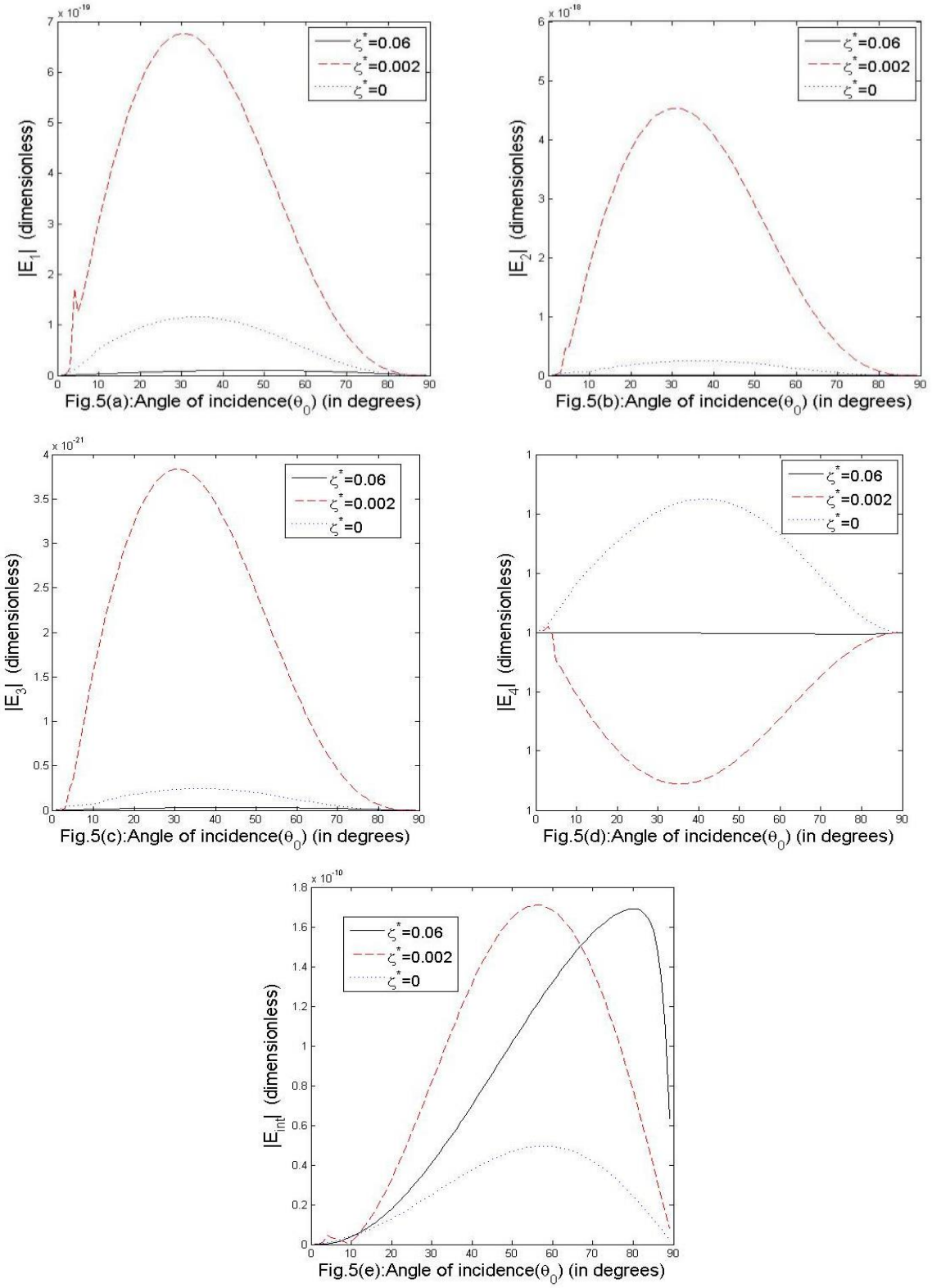


Fig. 5. Energy ratios of reflected wave w.r.t. angle of incidence ((a) $|E_1|$, (b) $|E_2|$, (c) $|E_3|$, (d) $|E_4|$, (e) $|E_{int}|$) for incident SV-wave at ς^*=0, 0.002, 0.06

T-wave

Figure 3 reveals the variation in energy ratios for distinct values of ς^* when T-wave is incident. Figure 3(a) shows that $|E_1|$ increase with angle of incidence as well as for higher

values of ς^*. On contrary to that $|E_2|$ decrease with angle of incidence and its values are reduced for higher values of ς^*. The values of $|E_3|$ and $|E_4|$ increase with angle of incidence but it follows adverse relation for higher values of ς^*. The values of $|E_{int}|$ decrease for higher values of θ in case of HTT and 1T model, whereas for TT model it increases with angle of incidence and dominates the region.

Ps-wave

When Ps-wave is incident the energy ratios for distinct values of ς^* are depicted with aid of Fig. 4. Figure 4(a) reveals that $|E_1|$decrease with angle of incidence for HTT and 1T models whereas for TT model it oscillates with higher values of θ dominates the entire range. The values of $|E_2|$ decrease for distinct considered cases. As observed in Fig. 3, here also TT values dominate the outcomes of other cases. The magnitude values of $|E_3|$ is of oscillatory nature in case of 1T and HTT models, whereas TT values increase with angle of incidence. It is also observed that magnitude values remain near to one for distinct models considered and angle of incidence. $|E_4|$ decrease for higher values of θ. The values attained for HTT and TT models are close to each other. Initially values of 1T are highest, but greater values of θ it has lowest values in the range. Figure 4(e) shows that $|E_{int}|$ has approximately same values for HTT and 1T cases, but for TT model its values are least and oscillatory in nature.

SV-wave

The behavior of energy ratios at distinct values of ς^* due to incidence of SV waves is demonstrated with help of Fig. 5. Energy ratios $|E_1|$ and $|E_2|$ are of oscillatory behavior as observed through Fig. 5(a,b). It initially increases with angle of incidence, attains highest value and then starts decreasing. It is also observed that TT values overcome the other cases and HTT values are least in the region. As observed in previous figures the values of $|E_3|$ is of oscillatory nature and the outcomes of 1T remain with the values acquired for HTT and TT models. $|E_4|$ has values approximately equal to one for the three cases considered. It is noticed that in case of HTT values are stationary whereas TT and 1T cases have oscillatory values in the region. On contrary to the trend of previous figures observations here TT values are least in the region.$|E_{int}|$ increases for initial values of θ, acquires highest value and then decreases. The values obtained for 1T model are least in the entire region.

Analysis of RGL and SGL model

An analysis based on the values of energy ratios acquired due to incidence of distinct waves for RGL and SGL models is represented with the help of Fig. 6–9.

P-wave

Figure 6(a) shows that P-wave is incident values of $|E_1|$ for RGL are higher than SGL model throughout the range. It is further noticed that RGL values are decreasing with angle of incidence, in contrast to that SGL values are increasing and remain close to one in entire

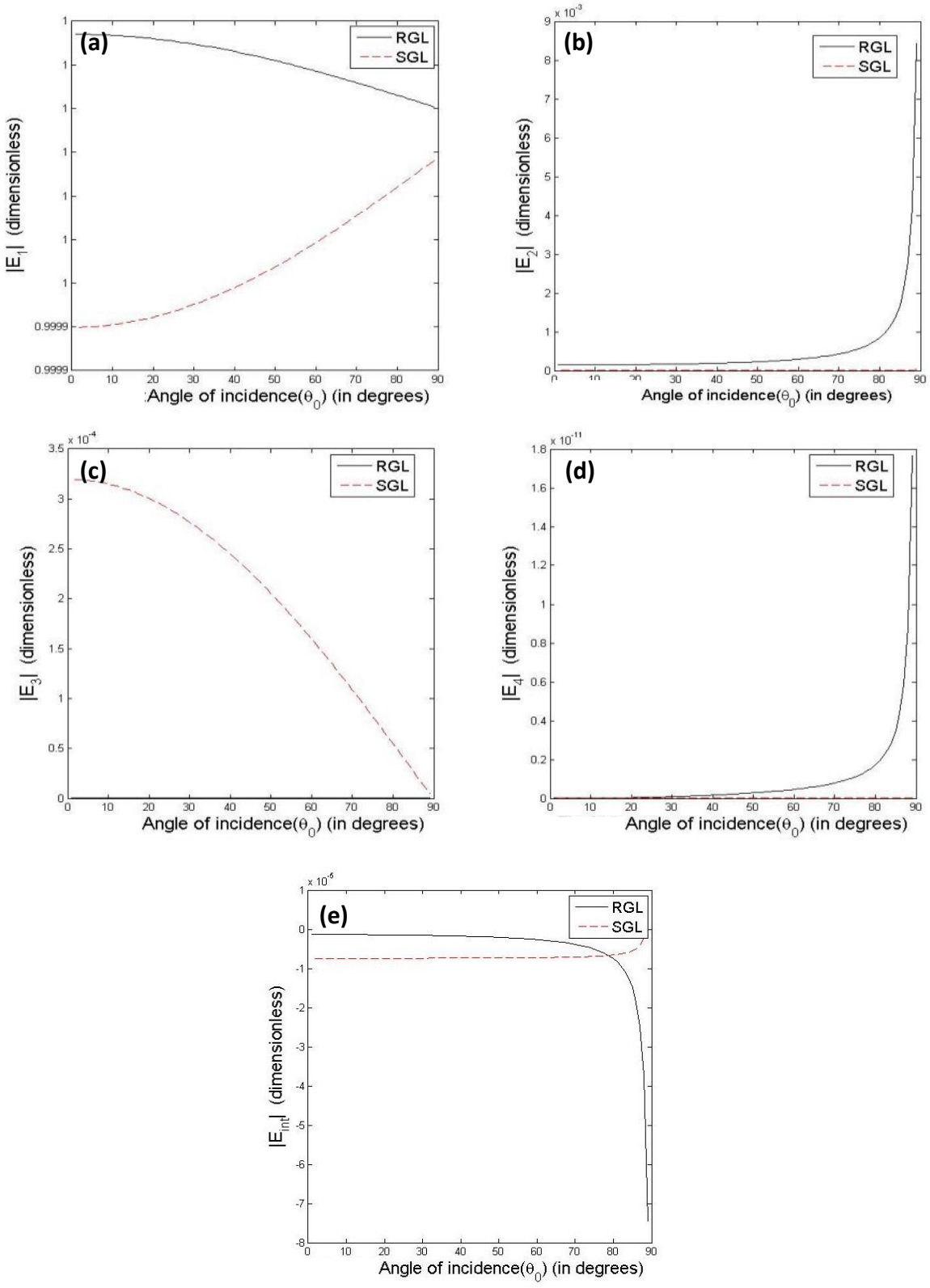


Fig. 6. Energy ratios of reflected wave w.r.t. angle of incidence ((a) $|E_1|$, (b) $|E_2|$, (c) $|E_3|$, (d) $|E_4|$, (e) $|E_{int}|$) for incident P-wave for the RGL and SGL models

range. $|E_2|$ is of increasing nature for both RGL and SGL models. As observed in Fig. 5, RGL values dominate the SGL model. Figure 6(c) depicts that trend of $|E_3|$ is of decreasing type and in this case SGL values are greater than RGL values at each angle of incidence.

The values of $|E_4|$increase with higher pace in case of RGL as observed with aid of Fig. 6(d). Figure 6(e) represents that $|E_{int}|$ varies in opposite manner in case of RGL and SGL models. RGL values keep decreasing whereas SGL values are increasing with angle of incidence.

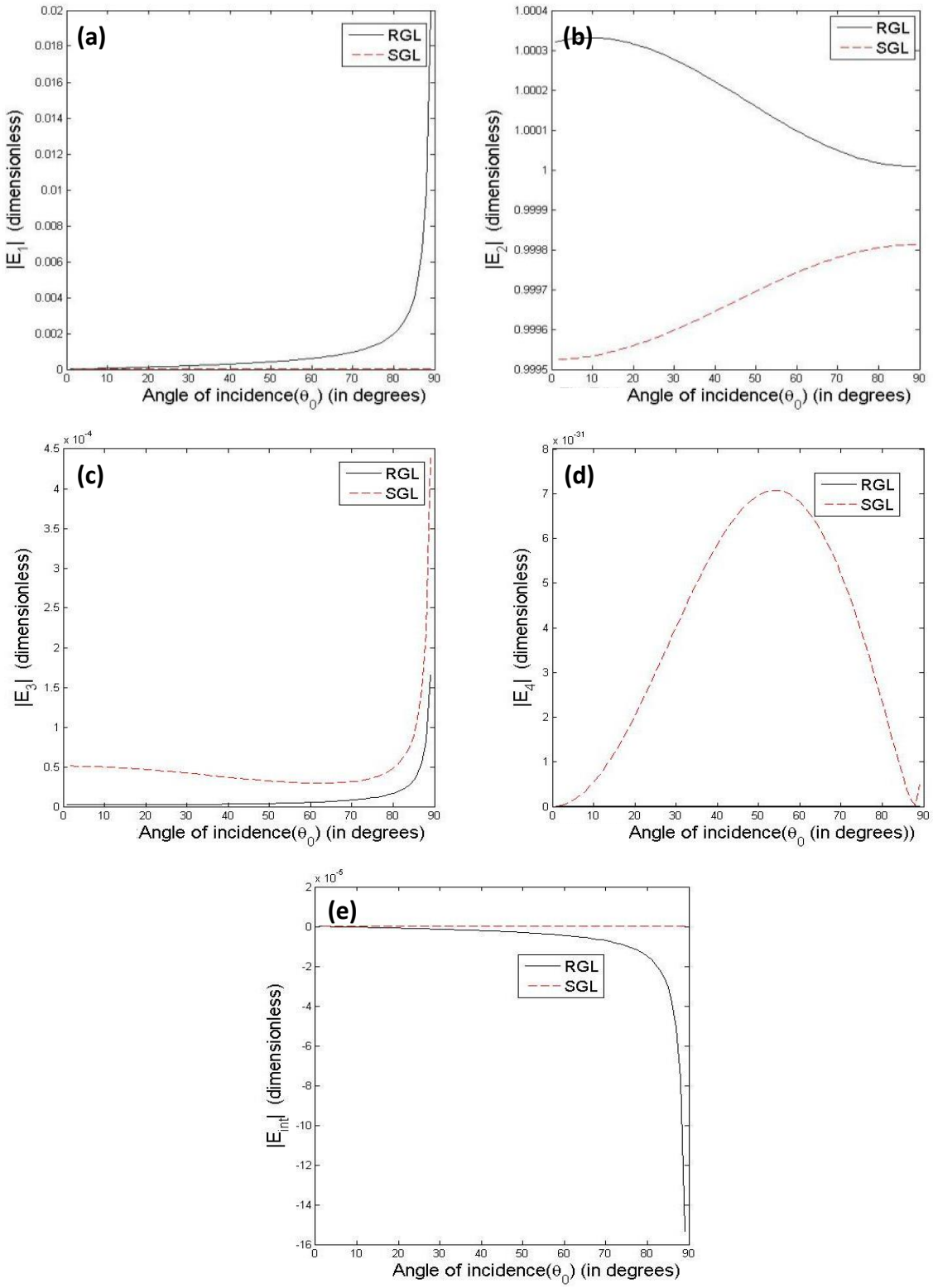


Fig. 7. Energy ratios of reflected wave w.r.t. angle of incidence
((a) $|E_1|$, (b) $|E_2|$, (c) $|E_3|$, (d) $|E_4|$, (e) $|E_{\text{int}}|$) for incident T-wave for the RGL and SGL models

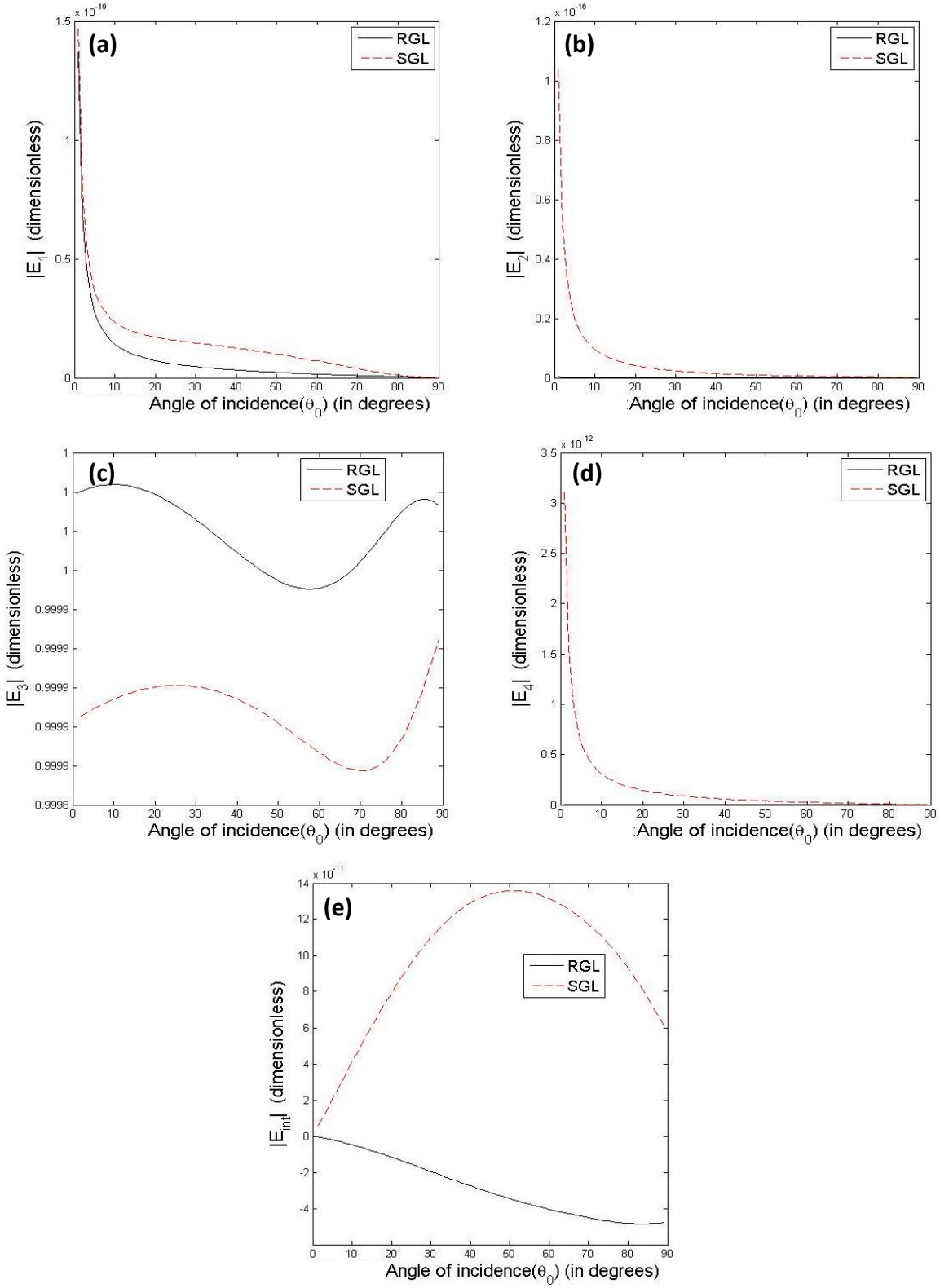


Fig. 8. Energy ratios of reflected wave w.r.t. angle of incidence ((a) $|E_1|$, (b) $|E_2|$, (c) $|E_3|$, (d) $|E_4|$, (e) $|E_{int}|$) for incident Ps-wave for the RGL and SGL models

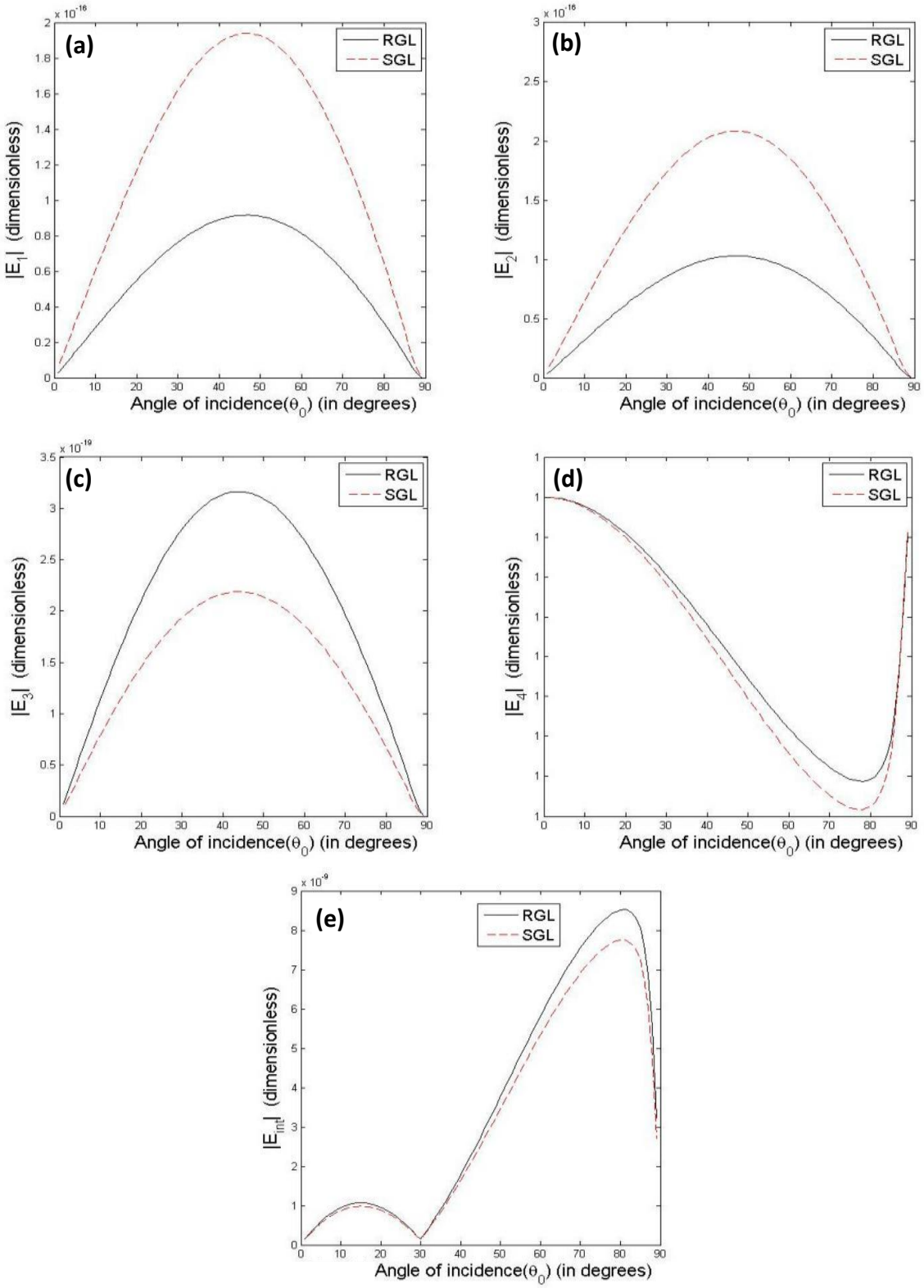


Fig. 9. Energy ratios of reflected wave w.r.t. angle of incidence ((a) $|E_1|$, (b) $|E_2|$, (c) $|E_3|$, (d) $|E_4|$, (e) $|E_{\text{int}}|$) for incident SV-wave for the RGL and SGL models

T-wave

The fluctuation in values of energy ratios due to incidence of T-wave in RGL and SGL models are demonstrated with the help of Fig. 7. Through Fig. 7(a) it is noticed that $|E_1|$

increases with angle of incidence in both RGL and SGL cases. But values of RGL are higher than the SGL throughout the range. The values of $|E_2|$ decrease in RGL model whereas for SGL model it increases and remain less the RGL values in complete range. An increasing trend in values of $|E_3|$ is noticed with the help of Fig. 7(c). In this case SGL values overcome RGL values. Oscillation behavior of $|E_4|$ is observed in case of RGL and SGL model. As observed in Fig. 6, here also SGL values are much higher than RGL values in entire range. A slight variation in magnitude values of $|E_{int}|$ is noticed in case of SGL, whereas RGL values keep decreasing and are less the SGL values in whole range.

Ps-wave

The variation in values of energy ratios due to incidence of Ps-wave in RGL and SGL models are depicted in Fig. 8. Figure 8(a) shows that outcomes $|E_1|$ diminishes with angle of incidence for both the cases. The results of SGL are higher than RGL model in complete range. The values of $|E_2|$ decrease with angle of incidence. As observed in Fig. 7, here also RGL values are lower than SGL values throughout the range. The values of $|E_3|$ keep fluctuating in whole range. In this case RGL dominates the outcomes of SGL model and remains near to one at each angle of incidence. $|E_4|$ has diminishing values with respect to angle of incidence in both the models considered. The values attained for RGL model are much less as compared to SGL model. $|E_{int}|$follows opposite trend for SGL and RGL models. In case of RGL model it initially decreases and then starts increasing, whereas for SGL model it initially increases with angle of incidence and then starts decreasing.

SV-wave

Figure 9 illustrates the variation in energy ratios when SV wave is incident. From Fig. 9(a), it is seen that values of $|E_1|$ are of oscillatory behavior in RGL and SGL models. It initially increases with angle of incidence obtains highest value at $\theta = 55°$ and then its value starts diminishing. It is also observed that in case of RGL model values remain less than SGL model throughout the range. Energy ratios $|E_2|$ is also of oscillatory nature and has highest value for SGL model as depicted in Fig. 9(b). On contrary to that the values of $|E_3|$ obtain greater values in case of RGL model. Figure 9(d) represents that values of $|E_4|$ are close to one at each angle of incidence for RGL and SGL model and outcomes of RGL overcome the SGL values in entire range. $|E_{int}|$ has oscillatory nature in entire nature as depicted in Fig. 9(e), here also RGL has higher values than SGL model in complete range.

Conclusion

In the present work, the reflection of plane waves in a porous thermoelastic half-space incorporating hyperbolic two-temperature effects has been investigated within the framework of the refined Green-Lindsay thermoelastic model. The analysis confirms the existence of three longitudinal waves (P-, T-, and Ps-waves) and one transverse SV-wave propagating with different velocities *ij* of the porous thermoelastic medium. Reflection coefficients corresponding to the incidence of each wave were derived, and the associated energy ratios were evaluated for the hyperbolic two-temperature (HTT), two-temperature (TT), and one-temperature (1T) models. Furthermore, the behaviour of energy ratios was examined for both refined Green-Lindsay (RGL) and simple Green-Lindsay (SGL) formulations.

Quantitative behavior of energy ratios

The numerical results demonstrate that the distribution of reflected wave energy strongly depends on the angle of incidence and the thermoelastic model considered in particular, the HTT formulation generally produces higher reflected energy ratios compared with the TT and classical 1T models for several incidence conditions, indicating the significant influence of hyperbolic thermal effects on wave reflection characteristics. The comparison between RGL and SGL models further shows that the RGL model yields more refined predictions due to the incorporation of additional thermal relaxation mechanisms.

Physical interpretation

From a physical standpoint, the hyperbolic two-temperature theory introduces finite thermal propagation speed and relaxation effects, which modify the coupling between thermal and elastic fields. Consequently, the HTT model improves the stability of thermoelastic wave propagation and alters the energy transmission behavior in porous thermoelastic media. Conservation of energy is satisfied for all angles of incidence, confirming the physical consistency of the obtained results.

Future research directions

The present analysis may provide useful insights into wave propagation phenomena in porous geotechnical materials such as soils and sedimentary rocks. Future work may extend the present formulation to more generalized models, including fraction order thermoelastic theories, anisotropic porous media, and rotating thermoelastic systems, to better capture wave interactions in complex geophysical and engineering environments.

Physical and engineering implications

The results obtained in the present study have important implications for wave propagation in porous geotechnical materials such as soil, sedimentary rocks, and fluid-saturated porous structures. The presence of hyperbolic two-temperature effects modifies the energy transmission characteristics of thermoelastic waves by introducing finite thermal propagation speed and relaxation effects. These phenomena can significantly influence wave reflection behavior in subsurface environments, which is important in geophysical exploration, earthquake engineering, and soil dynamics.

Furthermore, the interaction between pore pressure, thermal diffusion, and elastic deformation may affect energy dissipation and wave attenuation in porous materials, making the present model useful for studying thermoelastic effects in soil-structure interaction problems and subsurface energy transport.

Validation with existing studies

The qualitative behavior of the energy ratios obtained in this study is consistent with previously reported results on thermoelastic and poroelastic wave propagation in generalized thermoelastic media [38–41]. The observed variation of energy ratios with respect to the angle of incidence and thermal parameters agrees with earlier theoretical findings.

CRediT authorship contribution statement

Sharma Saurav: conceptualization, data curation, investigation; **Batra Divya**: investigation, data curation, writing-review and editing-original draft; **Kumar Rajneesh**: conceptualization, supervision, data curation.

Conflict of interest

Authors declare that they have no conflict of interest.

References

1. Biot MA. Theory of propagation of elastic waves in a fluid-saturated porous solid. I. Low frequency range. *The Journal of the Acoustical Society of America.* 1956;28(2): 168–178.
2. Biot MA. Theory of propagation of elastic waves in a fluid-saturated porous solid. II. Higher frequency range. *The Journal of the Acoustical Society of America.* 1956;28(2): 179–191.
3. Biot MA. Thermoelasticity and irreversible thermodynamics. *J. Appl. Phys.* 1956;27(3): 240–253.
4. Lord H, Shulman Y. A generalized dynamical theory of thermoelasticity. *J. Mech. Phys. Solids.* 1967;15(5): 299–309.
5. Green AE, Lindsay KA. Thermoelasticity. *J Elasticity.* 1972;2: 1–7.
6. Jabbari M, Dehbani H. An Exact Solution for Classic Coupled Thermoporoelasticity in Cylindrical Coordinates. *Journal of Solid Mechanics.* 2009;1(5): 343–357.
7. Jabbari M, Dehbani H. An Exact Solution for Lord-Shulman Generalized Coupled Thermoporoelasticity in Spherical Coordinates. *Journal of Solid Mechanics.* 2010;2(3): 214–230.
8. Eringen AC. Nonlocal polar elastic continua. *Int. J. Eng. Sci.* 1972;10(1): 1–16.
9. Eringen AC. Plane waves in nonlocal micropolar elasticity. *Int. J. Eng. Sci.* 1984;22(8–10): 1113–1121.
10. Erbay S, Erbay HA, Dost S. Nonlinear wave interactions in a micropolar elastic medium. *Wave Motion.* 1992;16(2): 163–172.
11. Jun W, Dhaliwal RS. On some theorems in the nonlocal theory of micropolar elasticity. *Int. J. Solids Struct.* 1993;30(10): 1331–1338.
12. Lazar M, Kirchner HOK. The Eshelby tensor in nonlocal elasticity and in nonlocal micropolar elasticity. *J. Mech. Mater. Struct.* 2006;1: 325–337.
13. Zeng Chen Y, Lee JD. Determining material constants in nonlocal micromorphic theory through phonon dispersion relations. *Int. J. Eng. Sci.* 2006;44(18–19): 1334–1345.
14. Najafi Eghtesad M, Daneshmand F. Boundary stabilization of vibration of nonlocal micropolar elastic media. *Appl. Math. Model.* 2012;36(8): 3447–3453.
15. Sharma K, Marin M. Effect of distinct conductive and thermodynamic temperatures on the reflection of plane waves in micropolar elastic half-space. *University Politehnica of Bucharest Scientific Bulletin-Series A-Applied Mathematics and Physics.* 2013;75(2): 121–132.
16. Sharma K, Marin M. Reflection and transmission of waves from imperfect boundary between two heat conducting micropolar thermoelastic solids. *Analele ştiinţifice ale Universităţii" Ovidius" Constanţa. Seria Matematică.* 2014;22(2): 151–176.
17. Sharma S, Sharma K. Influence of Heat Sources and Relaxation time on Temperature Distribution in Tissues. *International Journal of Applied Mechanics and Engineering.* 2014;19(2): 427–433.
18. Allam MNM, Rida SZ, Abo-Dahab SM, Mohamed RA, Kilany AA. GL model on reflection of P and SV waves from the free surface of thermoelastic diffusion solid under influence of the electromagnetic field and initial stress. *Journal of Thermal Stresses.* 2014;37(4): 471–487.
19. Abo-Dahab SM. Magnetic field effect on three plane waves propagation at interface between solid-liquid media placed under initial stress in the context of GL model. *Applied Mathematics & Information Sciences.* 2015;9(6): 3119.
20. Othman MIA, Ahmed EAA. Influence of the gravitational field on a piezothermoelastic rotating medium with GL theory. *The European Physical Journal Plus.* 2016;131(10): 358.
21. Lotfy Kh, Gabr ME. Response of a semiconducting infinite medium under two temperature theory with photothermal excitation due to laser pulses. *Optics & Laser Technology.* 2017;97: 198–208.
22. Abo-Dahab SM. Reflection of generalized magneto-thermoelastic waves with two temperatures under influence of thermal shock and initial stress. *Journal of Heat Transfer.* 2018;140(10): 102005.
23. Abo-Dahab SM, Lotfy Kh, Al-Juboori U. Reflection waves problem in a generalized thermoelastic half-space with two temperature and rotation. *African Journal of Engineering Research.* 2019;7(2): 33–44.

24. Saeed T, Abbas I, Marin M. A GL model on thermo-elastic interaction in a poroelastic material using finite element method. *Symmetry*. 2020;12(3): 488.
25. Anya AI, Khan A. Reflection and propagation of magneto-thermoelastic plane waves at free surfaces of a rotating micropolar fibre-reinforced medium under GL theory. *International Journal of Acoustics and Vibration*. 2020;25(2): 190–199.
26. Kalkal KK, Devender S, Sunita D. Reflection of plane waves in a nonlocal micropolar thermoelastic medium under the effect of rotation. *Acta Mechanica*. 2020;231: 2849–2866.
27. Sharma S, Khator S. Power generation planning with reserve dispatch and weather uncertainties including penetration of renewable sources. *International Journal of Smart Grid and Clean Energy*. 2021;10(4): 292–303.
28. Sharma S, Khator S. Micro-Grid planning with aggregator's role in the renewable inclusive prosumer market. *Journal of Power and Energy Engineering*. 2022;10(4): 47–62.
29. Abouelregal AE, Sedighi HM. Elastic Thermal Deformation of an Infinite Copper Material Due to Cyclic Heat Supply Using Higher-Order Nonlocal Thermal Modeling. *Metals*. 2022;12(11): 1927.
30. Abouelregal AE. Response of thermoelastic cylindrical cavity in a non-local infinite medium due to a varying heat source. *Waves in Random and Complex Media*. 2022;32(4): 1725–1742.
31. Abouelregal AE. An advanced model of thermoelasticity with higher-order memory-dependent derivatives and dual time-delay factors. *Waves in Random and Complex Media*. 2022;32(6): 2918–2939.
32. Bibi F, Ali H, Azhar E, Jamal M, Ahmed I, Ragab AE. Propagation and reflection of thermoelastic wave in a rotating nonlocal fractional order porous medium under Hall current influence. *Scientific Reports*. 2023;13(1): 17703.
33. Punia BS, Deswal S, Kalkal KK, Othman MIA. Reflection of plane waves in an orthotropic micropolar thermoelastic diffusive medium with two-temperature. *Indian Journal of Physics*. 2021;98(2): 613–628.
34. Kaushal S, Kumar R, Bala I, Sharma G. Impact of non-local, two temperature and impedance parameters on propagation of waves in generalized thermoelastic medium under modified Green-Lindsay model. *Materials Physics and Mechanics*. 2024;52(1): 1–17.
35. Kumar D, Paswan B, Singh P, Chattopadhyay A. Reflection and transmission of plane wave at the interface between two distinct nonlocal triclinic micropolar generalized thermoelastic half spaces under DPL and LS theory. *Acta Mechanica*. 2024;235(5): 3245–3270.
36. Abouelregal AE, Nasr ME, Muaz U, Abouhawwash M, Khalil KM. Micropolar viscoelastic nanostructures subjected to laser-induced heat flux using the modified higher-order thermoelasticity model incorporating phase delay effects. *Acta Mech*. 2024;235: 4119–4140.
37. Sharma S, Batra D, Kumar R. Fractional strain analysis on reflection of plane waves at an impedance boundary of non-local swelling porous thermoelastic medium. *Materials Physics and Mechanics*. 2025;53(1): 1–21.
38. Sharma S, Batra D, Kumar R. Waves in porothermoelastic half space at impedance boundary with three phase lag delays. *Journal of Vibration Engineering & Technologies*. 2025;13(5): 277.
39. Sharma S, Marin M, Altenbach H. Elastodynamic interactions in thermoelastic diffusion including non-local and phase lags. *ZAMM Journal of Applied Mathematics and Mechanics*. 2025;105(1): e202401059.
40. Marin M, Sharma S, Kumar R, Vlase S. Fundamental solution and Green's function in orthotropic photothermoelastic media with temperature-dependent properties under the Moore–Gibson–Thompson model. *Z Angew Math Mech*. 2025;105**:** e70124.
41. Kumar R, Marin M, Vlase S. The effect of viscosity on energy ratios in elastic materials with piezoelectric properties considering two temperature levels and a three-phase lag. *Mech. Solids*. 2025;60: 2033–2047.
42. Abouelregal AE, Marin M, Öchsner A. A modified spatiotemporal nonlocal thermoelasticity theory with higher-order phase delays for a viscoelastic micropolar medium exposed to short-pulse laser excitation. *Continuum Mechanics and Thermodynamics*. 2025;37: 15.
43. Abouelregal AE, Marin M, Foul A, Askar SS. Nonlocal micropolar thermoelastic half-space: a higher-order model incorporating phase lags and nonlocal effects in space and time. *Appl. Phys. A*. 2025;131: 248.
44. Abouelregal AE, Marin M, Alhassan Y, Atta D. A novel space–time nonlocal thermo-viscoelastic model with two-phase lags for analyzing heat diffusion in a half-space subjected to a heat source. *Iranian Journal of Science and Technology, Transactions of Mechanical Engineering*. 2025;49: 1315–1332.
45. Abouelregal AE, Marin M, Abdelaziz F, Sameh SA. Space-time non-local analysis of a porous thermoelastic hollow cylinder using a heat conduction model featuring a Goufo-Caputo two-parameter fractional derivative with phase lags. *Boundary Value Problems*. 2025;2025: 29.
46. Tiersten HF. Elastic surface waves guided by thin films. *J. Appl Phys*. 1969;40(2): 770–789.
47. Malischewsky PG. *Surface waves and Discontinuities*. Amsterdam: Elsevier; 1987.
48. Achenbach JD. *Wave propagation in elastic solids*. North Holland, Amsterdam: IST; 1973.